PERGAMON

Journal of Structural Geology 22 (2000) 993–1008

JOURNAL OF STRUCTURAL GEOLOGY

www.elsevier.nl/locate/jstrugeo

Progressive development of mantle structures around elongate porphyroclasts: insights from numerical models

Nibir Mandal[a], Susanta Kumar Samanta[a], Chandan Chakraborty[b,*]

[a]*Department of Geological Sciences, Jadavpur University, Calcutta 700032, India*
[b]*Geological Studies Unit, Indian Statistical Institute, 203 B.T. Road, Calcutta 700035, India*

Received 30 August 1999; accepted 2 March 2000

Abstract

This paper presents a generalized theoretical approach towards two-dimensional numerical modeling of the mantle geometry of inequant porphyroclasts of varying shapes within a Newtonian matrix during progressive, general type of bulk deformation. The analysis takes into account the effects of synkinematic size reduction of the porphyroclast with concomitant mantle development in response to dynamic recrystallization. Numerical simulations reveal that the principal factors governing the geometry of mantle structures are: (1) the initial aspect ratio of the porphyroclast (a/b), (2) the rate of clast-size reduction, and (3) the ratio of the rates of pure shear and simple shear (S_r) or the kinematic vorticity (W_k) in the general type of non-coaxial deformation. In general, porphyroclasts develop δ-, ϕ- and finally, σ-type mantle structures, as the rate of clast-size reduction is progressively increased. The tails of equant porphyroclasts tend to be characterized by wings with increase in bulk shear during progressive deformation. In contrast, inequant objects ($a/b > 1$) develop composite tails with multiple wings, even at low finite shear strains. However, with increase in aspect ratio δ geometry tends to dominate the overall mantle structure. Porphyroclasts with a large aspect ratio ($a/b = 3$) form tails with overturned δ-wings, as described in Passchier, C.W., Simpson, C., 1986. "Porphyroclast system as kinematic indicators", Journal of Structural Geology 8, 831–844. In general the type of non-coaxial deformation, with decrease in kinematic vorticity (or increase in S_r), porphyroclasts irrespective of their initial shapes, tend to form atypical δ-like tails that do not cross the central reference plane.

1. Introduction

Following the key publication by Passchier and Simpson (1986), mantled porphyroclast systems have increasingly gained importance in the kinematic analysis of deformed rocks (Choukroune et al., 1987; Mawer, 1987; Van Den Driessche and Brun, 1987; Hooper and Hatcher, 1988; Bjornerud, 1989; Hanmer and Passchier, 1991; Simpson and De Paor, 1993). Recent studies have revealed that the evolution of different types of mantled porphyroclasts, e.g. δ-type, σ-type, etc, is itself a subject requiring more detailed consideration (Passchier et al., 1993; Passchier, 1994; Bjornerud and Zhang, 1995; Masuda and Mizuno, 1996). Passchier et al. (1993) and Passchier (1994) have provided genetic models for the development of mantle structures in relation to the flow perturbation around rigid porphyroclasts. The flow perturbation that is mainly of two types, with an eye-shaped and a bow-tie shaped separatrix, is sensitive to the viscous rheology (Newtonian or non-Newtonian) of the matrix. Passchier (1994) has comprehensively classified mantled porphyroclasts into four types (θ-, δ-, ϕ- and σ-type), and explained their development by considering the position of the initial mantle relative to the flow separatrix.

The mantle structures of porphyroclasts have been successfully simulated in experiments with Newtonian as well as non-Newtonian matrix (Passchier and Simpson, 1986; ten Brink and Passchier, 1995; Passchier

* Corresponding author.
E-mail addresses: nibir@jugeo.clib0.ernet.in (N. Mandal), chandan@isical.ac.in (C. Chakraborty).

0191-8141/00/$ - see front matter
PII: S0191-8141(00)00020-1

and Sokoutis, 1993). The experimental results apparently conform to the theoretical genetic models, formulated on the basis of the geometry of flow perturbations around rigid porphyroclasts (Passchier, 1994) barring some deviations (Masuda and Mizuno, 1996). In addition, they provide a volume of information about how the mantle structures of porphyroclasts change their geometry in the course of progressive deformation to a large finite strain.

Numerical simulation (ten Brink et al., 1993; Bjornerud and Zhang, 1995; Masuda and Mizuno, 1996) is another useful approach to studying the evolution of mantled porphyroclasts. This approach has some advantages, as one can simulate a structure over a large finite strain in a parallel-sided shear zone, while imposing a number of boundary conditions. Bjornerud and Zhang (1995) have determined the stability fields of common types of mantle structures by considering synkinematic size reduction of the spherical porphyroclast as a variable and a slip or non-slip condition at the matrix–porphyroclast interface. The model results are, however, restricted to moderate finite shear strains ($\gamma < 10$). Natural as well as experimental observations (ten Brink and Passchier, 1995) indicate that the evolution of a porphyroclast may involve a large finite strain, giving rise to additional complexities in the mantle structure. This is also evident from the numerical models of Masuda and Mizuno (1996) where they have analyzed mantled porphyroclasts in both a Newtonian and a non-Newtonian matrix by varying the initial mantle width. In contrast to Bjornerud and Zhang (1995) model, their model, however, considers a fixed dimension of the object in the progressive deformation.

All these numerical models show the probable modes of development of mantle structure around *spherical* porphyroclasts in a *simple shear* type of progressive bulk deformation. However, in natural mylonites porphyroclasts are often elongate in shape (Passchier and Simpson, 1986). In addition, the bulk deformation can have a shortening component across the shear zone. In detail, the shapes of natural mantled porphyroclasts are thus likely to be more complex and to deviate from those so far predicted by simulations with objects of equant shape and progressive simple shear (Passchier and Trouw, 1996). In this paper we present a more generalized two-dimensional theoretical model, and show probable patterns of mantle structure around elongate porphyroclasts in a Newtonian matrix. This model, when applied to equant clasts and simple shear type of progressive deformation, yields results similar to those of earlier models. We also show how the mantle structure can vary with the changing ratio of the rates of pure shear and simple shear in the shear zone, when all other factors remain unchanged.

2. Theoretical considerations

Existing numerical simulations (Bjornerud and Zhang, 1995; Masuda and Mizuno, 1996) enumerate the modes of development of mantle structure around equant porphyroclasts, which rotate with a constant velocity of $\dot{\gamma}/2$, where $\dot{\gamma}$ is the bulk shear strain-rate. The velocity field around such objects is derived by applying the mathematics of spherical harmonics (Lamb, 1932). Numerical modeling of elongate mantled porphyroclasts, on the other hand, requires determination of the velocity field around a non-spherical object that virtually rotates with a changing angular velocity in the course of progressive deformation. In such a situation, the rotation rate of the object, at any instant, would further be controlled by the shape and orientation of the object at that instant and the ratio between the rates of flattening and simple shear ($\dot{\varepsilon}/\dot{\gamma}$) in the general type of non-coaxial progressive deformation (Ghosh and Ramberg, 1976; Passchier, 1987). The velocity functions for an inequant object are thus more complex than those deduced for spherical objects (Masuda and Mizuno, 1996). Moreover, the velocity field outside the inequant object will also continuously change as the object reorients itself in the course of progressive deformation. Numerical simulations of elongate mantled porphyroclasts thus demand a different mathematical approach.

Jeffery (1922) has given an elegant mathematical treatment on the motion of an ellipsoidal object embedded in a viscous medium. Considering an ellipsoidal coordinate system, with the origin at the center of the object, he obtains a solution of the Navier–Stokes' equation for viscous flow, and describes the instantaneous velocity field around the object. The velocity at a point is a function of the coordinate of that point, λ (ellipsoidal coordinate), with respect to the surface of the object, which is taken as the surface of reference ($\lambda = 0$). As the distance of points from the surface of the object becomes large, i.e. λ tends to infinity, the velocity tends to approach that of a homogeneous flow of the medium far away from the object. Jeffery's equations, determining the rate of rotation of an object in a laminar flow (his equation 41), have been utilized to analyze the kinematics of rigid inclusions within a ductile rock (Ghosh and Ramberg, 1976; Passchier, 1987). From his theory one can also obtain functions for the instantaneous velocity field outside the rigid object. However, utilizing these functions to derive the velocity field is complicated, as the functions have complex constants and parameters. Secondly, they are described with reference to the coordinate axes along the axial directions of the object, which themselves move during progressive deformation. Jezek et al. (1999) have circumvented these hurdles by solving velocity functions numerically with

the help of a computer program. In our analysis, instead, we have considered the velocity functions in two dimensions, [equations (22) and (23) of Jeffery, 1922] and analytically derived the expressions for the constant terms in the functions with respect to a fixed reference by satisfying boundary conditions. The terms finally came out in much simpler forms (details in Appendix A).

The development of mantled porphyroclasts takes place by accumulation of a large finite strain, involving a large rotation of the porphyroclast (Passchier and Simpson, 1986). We therefore deal with a moving reference $0x'y'$, and a fixed reference $0xy$ with the origins at the center of the object (Fig. 1). The axes of the former reference are chosen to remain always in coincidence with the axial directions of the object, which thereby rotate in concert with the object sweeping through different material lines. The fixed reference, $0xy$, is chosen to describe the bulk deformation tensor. The surface of the elongate object can be simply represented with respect to the moving reference, $0x'y'$, as: $x'^2/a^2+y'^2/b^2=1$. The rotation of the object takes place about the z'-axis, which is assumed to coincide with the z-axis; here the direction of no strain. At any instant the displacement at a point (x, y) in the neighborhood of the object is computed along the following steps. (1) As shown later, the velocity functions [Eq. (10a)] are expressed with respect to the rotating reference frame $(0x'y')$; therefore, we first need to make a coordinate transformation from (x, y) to (x', y') to obtain the velocity vector; (2) the velocity vector with respect to the fixed reference frame $0xy$, is then obtained by a tensorial transformation of the vector derived in step 1; (3) the velocity vector in the next increment is derived in the same way as stated in step 1, but after rotating the $0x'y'$ reference frame, to be in coincidence with the axial directions of the object in its new position. These steps are then repeated to trace the movement of the point at every instant of progressive incremental deformation. Before going into the details of numerical simulations of mantle structures of porphyroclasts by this method, we shall introduce our mathematical formulation briefly in the main text. Details are given in Appendix A.

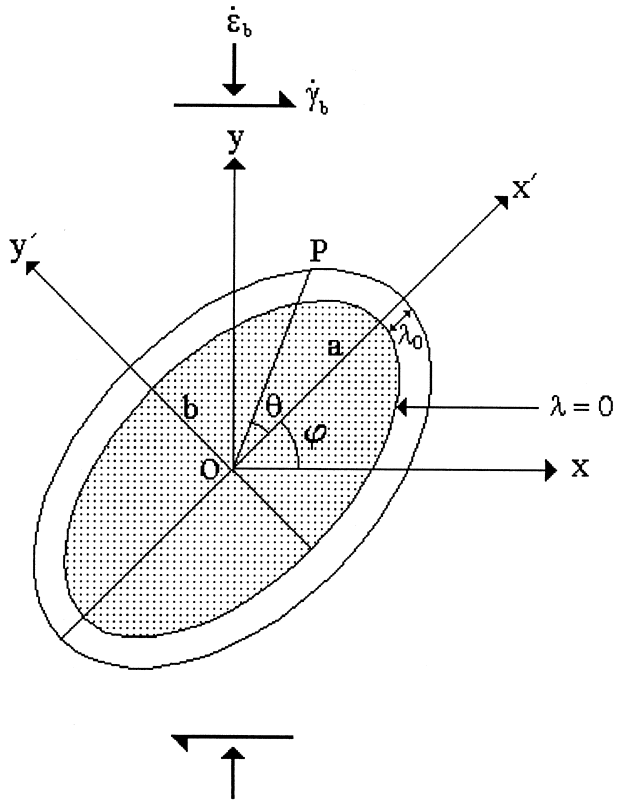

Fig. 1. Geometrical and kinematic considerations for the theoretical analysis. $0xy$ and $0x'y'$ are stationary and moving coordinate frames, respectively, with x- and x'-axis parallel to the bulk shear direction and along the long axis of the elliptical object. λ_0 = the distance of initial mantle boundary from the boundary of object. ϕ is the inclination of the long axis of object with the bulk shear direction and θ is the polar coordinate of a point (P) on the mantle boundary with respect to the x'-axis. $\dot{\gamma}_b$ and $\dot{\varepsilon}_b$ are the rates of bulk shear and shortening perpendicular to the bulk shear direction, respectively.

2.1. Mathematical derivation

Let us consider that the object is hosted in an infinitely extended viscous medium. Far away from the object, the medium is subjected to a shear flow at a rate, $\dot{\gamma}_b$, with a flattening rate of $\dot{\varepsilon}_b$, at right angles to the shear direction. We set the fixed reference, $0xy$, with the x axis parallel to the shear direction. Let the long axis of the object at any instant makes an angle of ϕ with the shear direction (Fig. 1). Taking the reference, $0x'y'$, with the x' axis along the long axis of the object, the position of a point near the object can be expressed by an elliptic coordinate, λ, as:

$$\frac{x'^2}{a^2+\lambda}+\frac{y'^2}{b^2+\lambda}=1. \tag{1}$$

The velocity components in a two-dimensional slow viscous flow follow well-known Navier–Stokes' equation

$$\frac{\partial^2 u'}{\partial x'^2}+\frac{\partial^2 u'}{\partial y'^2}-\frac{\partial p}{\partial x'}=0 \tag{2a}$$

$$\frac{\partial^2 v'}{\partial x'^2}+\frac{\partial^2 v'}{\partial y'^2}-\frac{\partial p}{\partial y'}=0, \tag{2b}$$

assuming that the equation of continuity is satisfied and the flow does not involve any body forces. u' and v' are the velocity components along x' and y'-axis, respectively. p is the confining pressure at a point. From

the condition of continuity, we can write

$$\frac{\partial u'}{\partial x'} + \frac{\partial v'}{\partial y'} = 0. \tag{3}$$

The solution of Eqs. (2a) and (2b) will have to agree with the following velocity conditions at large distances from the origin ($\lambda \to \infty$) and the surface of the object ($\lambda = 0$), respectively:

$$u_0' = S_{11}'x' + S_{12}'y',\ v_0' = S_{21}'x' + S_{22}'y' \tag{4}$$

and

$$u_s' = -\omega y',\ v_s' = \omega x'. \tag{5}$$

S'_{ij} is the instantaneous bulk strain-rate tensor with respect to $x'y'$ coordinates. The bulk strain-rate tensor with respect to the fixed coordinates, xy, is:

$$S_{ij} = \begin{bmatrix} \dot{\varepsilon}_b & \dot{\gamma}_b \\ 0 & -\dot{\varepsilon}_b \end{bmatrix}. \tag{6}$$

From the rule of transformation of a second rank tensor, we have:

$$S'_{pq} = l_{ip}l_{jq}S_{ij} \tag{7}$$

l_{ij} is the tensor for coordinate transformation.

In our case, i.e. two-dimensional coordinate, we can write:

$$l_{ij} = \begin{bmatrix} \cos\varphi & -\sin\varphi \\ \sin\varphi & \cos\varphi \end{bmatrix}. \tag{8}$$

From Eqs. (6) and (8), the components of the instantaneous strain-rate tensor in Eq. (7) are obtained in terms of the component of S_{ij} as:

$$\begin{aligned} S_{11}' &= \dot{\gamma}_b\left(S_r\cos 2\varphi + \frac{1}{2}\sin 2\varphi\right)\ S_{22}' = -\dot{\gamma}_b\left(S_r\cos\right. \\ &\left.2\varphi + \frac{1}{2}\sin 2\varphi\right) S_{21}' = \dot{\gamma}_b\left(\cos^2\varphi - S_r\sin 2\varphi\right) \\ S_{12}' &= -\dot{\gamma}_b\left(\sin^2\varphi + S_r\sin 2\varphi\right). \end{aligned} \tag{9}$$

S_r is the ratio between pure shear rate and simple shear rate ($\dot{\varepsilon}_b/\dot{\gamma}_b$) in the bulk progressive deformation, and ω is the instantaneous angular velocity of the object.

Following Jeffery's approach a general solution of Eqs. (2a) and (2b) can be written as

$$\begin{aligned} u' = {} & S_{11}'\left[1 - 2A(\alpha+\beta) + F\gamma\right]x' + \frac{1}{2}\left(S_{12}' + S_{21}'\right) \\ & \times\left[2(\alpha D - \beta C) + E\gamma\right]y' + S_{12}'y' \\ & - \frac{2\Delta x'y'}{b'^2x'^2 + a'^2y'^2}\left[\frac{1}{2}\left(S_{12}' + S_{21}'\right)\right. \\ & \times\left\{\frac{E + 2a'^2C + 2b'^2D}{a'^2}\right\}x' \\ & \left. + S_{11}'\left\{\frac{F - 2a'^2A + 2b'^2B}{b'^2}\right\}y'\right] \end{aligned} \tag{10a}$$

and

$$\begin{aligned} v' = {} & -S_{11}'\left[1 - 2B(\alpha+\beta) - F\gamma\right]y' - \frac{1}{2}\left(S_{12}' + S_{21}'\right) \\ & \times\left[2(\alpha D - \beta C) - E\gamma\right]x' + S_{21}'x' \\ & - \frac{2\Delta x'y'}{b'^2x'^2 + a'^2y'^2}\left[\frac{1}{2}\left(S_{12}' + S_{21}'\right)\right. \\ & \times\left\{\frac{E + 2a'^2C + 2b'^2D}{b'^2}\right\}y' \\ & \left. - S_{11}'\left\{\frac{F - 2a'^2A + 2b'^2)B}{a'^2}\right\}x'\right] \end{aligned} \tag{10b}$$

where $a' = \sqrt{a^2 + \lambda}$, $b' = \sqrt{b^2 + \lambda}$ and $\Delta = a'b'$

α, β and γ are geometric parameters, whose expressions in two-dimensions can be written as

$$\alpha = \int_\lambda^\infty \frac{d\lambda}{a'^2\Delta},\ \beta = \int_\lambda^\infty \frac{d\lambda}{b'^2\Delta},\ \gamma = \int_\lambda^\infty \frac{d\lambda}{a'^2b'^2\Delta}. \tag{11}$$

Solving the integrals in Eq. (11) (derivations in Appendix A), we have

$$\alpha = \frac{2}{(a^2 - b^2)}\left[\frac{a' - b'}{a'}\right],\ \beta = \frac{2}{(a^2 - b^2)}\left[\frac{a' - b'}{b'}\right],$$

$$\gamma = \frac{2}{(a^2 - b^2)^2}\left[\frac{(a' - b')^2}{a'b'}\right].$$

From Eqs. (A6), (A7) and (A8) in Appendix A the expressions of the constant parameters in Eqs. (10a) and (10b) are derived into simple forms as:

$$A = \frac{(a+b)^2}{8},\ B = -\frac{(a+b)^2}{8},$$

$$C = \frac{ab(a+b)^2}{4(a^2+b^2)}, D = \frac{ab}{4}\left(\frac{a-b}{a^2+b^2}\right)^2,$$

$$E = -\frac{ab}{4}\frac{(a+b)^2}{2},\ F = \frac{a^2+b^2}{4}.$$

In Eq. (10a) λ, one of the elliptical coordinates of

the point has a relation with the Cartesian coordinates as:

$$\lambda = \frac{1}{2}\left\{\left(x'^2 + y'^2\right) - \left(a^2 - b^2\right) + \sqrt{\left(x'^2 + y'^2 - a^2 - b^2\right) - 4\left(a^2b^2 - bx'^2 - ay'^2\right)}\right\}. \quad (12)$$

Now, to find the instantaneous velocity components at a point (x, y) we first have to make the following coordinate transformation:

$$\begin{bmatrix} x' \\ y' \end{bmatrix} = \begin{bmatrix} x \\ y \end{bmatrix}\begin{bmatrix} \cos\varphi & \sin\varphi \\ -\sin\varphi & \cos\varphi \end{bmatrix}$$

and determine the velocity components from Eqs. (10a) and (10b). Finally, the velocity field with respect to the fixed reference, $0xy$, is obtained by a reverse transformation:

$$\begin{bmatrix} u \\ v \end{bmatrix} = \begin{bmatrix} u' \\ v' \end{bmatrix}\begin{bmatrix} \cos\varphi & -\sin\varphi \\ \sin\varphi & \cos\varphi \end{bmatrix}. \quad (13)$$

The velocity at a point (x, y) will depend on the position of the point with respect to the object boundary ($\lambda = 0$) in Eq. (1). This can be determined by taking the sign of λ from Eq. (12). $\lambda > 0$ indicates that the point occurs outside the object boundary, while $\lambda = 0$ and $\lambda < 0$ indicate that the points lie on the surface and inside the object, respectively. At an instant, points lying outside the object, will move with velocity components as in Eq. (13), while points either on the surface or inside the object will move with velocity components:

$u = -\omega y$ and $v = \omega x$,

ω is the instantaneous angular velocity of the object. We can simplify Eq. (A8) and get,

$$\omega = -\frac{a^2\left(\sin^2\varphi + S_r \sin 2\varphi\right) + b^2\left(\cos^2\varphi - S_r \sin 2\varphi\right)}{a^2 + b^2}\dot{\gamma}_b. \quad (14)$$

From Eqs. (10a), (10b) and (12) we can now establish the instantaneous velocity field when the bulk strain-rate tensor in Eq. (6) is specified. It may be noted that the parameters, A, B, C, in Eqs. (10a) and (10b) are functions of object's dimensions, a and b. We consider that the object gets reduced in size at a rate of $\dot{R}_a$ and $\dot{R}_b$ along its a and b axial directions, respectively. All the constants in Eqs. (10a) and (10b) and the elliptical coordinate, λ in Eq. (12) will thus change at every instant. Numerical simulations of the changing velocity field were made in the following way.

2.2. Simulations of tail structures

Following the conventional method we have simulated numerically the geometric shapes of the mantle around porphyroclasts by imposing incremental strains in successive steps. Let us consider a contour around the porphyroclast, at a distance of λ_0, from the surface ($\lambda = 0$) of the porphyroclast delimiting the mantle from the matrix (Fig. 1). The Cartesian coordinates of any point on the contour are then,

$x'_0 = (a + \lambda_0)\cos\theta$ and $y'_0 = (b + \lambda_0)\cos\theta$,

where θ is the polar coordinate of the point with respect to the long axis of the porphyroclast. The distortion pattern of this elliptical contour during progressive deformation was determined by calculating incremental displacement from Eq. (13), with due consideration of changes in the axial dimensions and orientation of the object in each step of incremental deformation. With the help of a computer program in Visual Basic, we ran numerical experiments for a number of increments, and obtained the distortion patterns of the elliptical contour to simulate those observed in natural and experimental mantled porphyroclasts. Our numerical simulations attempt to investigate the control of the following factors on the development of tail structures: (1) the initial shape of the porphyroclast (represented by the aspect ratio a/b), (2) the rate of size reduction ($\dot{R}_a$, $\dot{R}_b$) of the porphyroclast, (3) the ratio between pure shear and simple shear rates in the bulk deformation (S_r) and (4) finite bulk shear strain. Numerical models that have been obtained by varying these factors are described in the following section. It may be noted that we shall express the rotationality of the bulk deformation by kinematic vorticity number W_k, where $W_k = 1/\sqrt{1 + 4S_r^2}$ (Ghosh, 1987).

3. Numerical models

The model of Passchier (1994) explains the principal types of mantle structures around porphyroclasts, based on the relative position of the initial mantle with respect to the flow separatrix around the rigid core. Under natural circumstances the rigid core continuously reduces its size due to dynamic recrystallization, adding new material to the mantle. As a consequence, the separatrix shrinks in the course of progressive deformation, giving rise to more complex structures (p. 375, Passchier, 1994). In this study we investigate the possible effects of the rate of size reduction of the porphyroclast ($\dot{R}$) and the kinematic vorticity (W_k) in the matrix, on the progressive development of mantle structures for large finite shear strain.

In the present discussion we need to refer to the fol-

lowing terms (Fig. 2) for the clarity of the description of mantle structures: *Mantle structure*—deformed geometry of the mantle around the rigid core of a porphyroclast. *Tails*—the portions of the deformed mantle on either side of the rigid core. *Wing*—narrow offshoots of a tail (Fig. 2a). *Branch Point*—the point from which a wing offshoots from the tail. *Wing migration*—the bodily migration of a wing along with the branch point (Fig. 2b). *Wing lengthening*—the increase in length of a wing, which occurs in two modes—(i) shifting of the branch point without wing stretching, (ii) wing stretching without branch point shifting (Fig. 2c). *Contractional face and extensional face*—portions of the object, at any instant, facing the contractional and extensional fields, respectively (Fig. 2a). *Side stepping*—refers to the lateral offset of the tails on either side of a porphyroclast (Fig. 2d).

3.1. Porphyroclasts with aspect ratio = 1

A series of numerical model experiments was performed by varying the rate of clast-size reduction, but keeping the bulk shear rate constant ($\dot{\gamma}_b = 0.025\ s^{-1}$). At a low rate of clast-size reduction (Fig. 3a; $\dot{R}_a = \dot{R}_b = 0.125$ unit/s, 1 unit $= 10^{-3}$ *a*) the mantle develops first generation δ-type tails, as observed in experiments (Passchier and Simpson, 1986) and in earlier numerical simulations (Bjornerud and Zhang, 1995; Masuda and Mizuno, 1996). With progressive deformation the first generation tails transform into wings (I in Fig. 3a) in

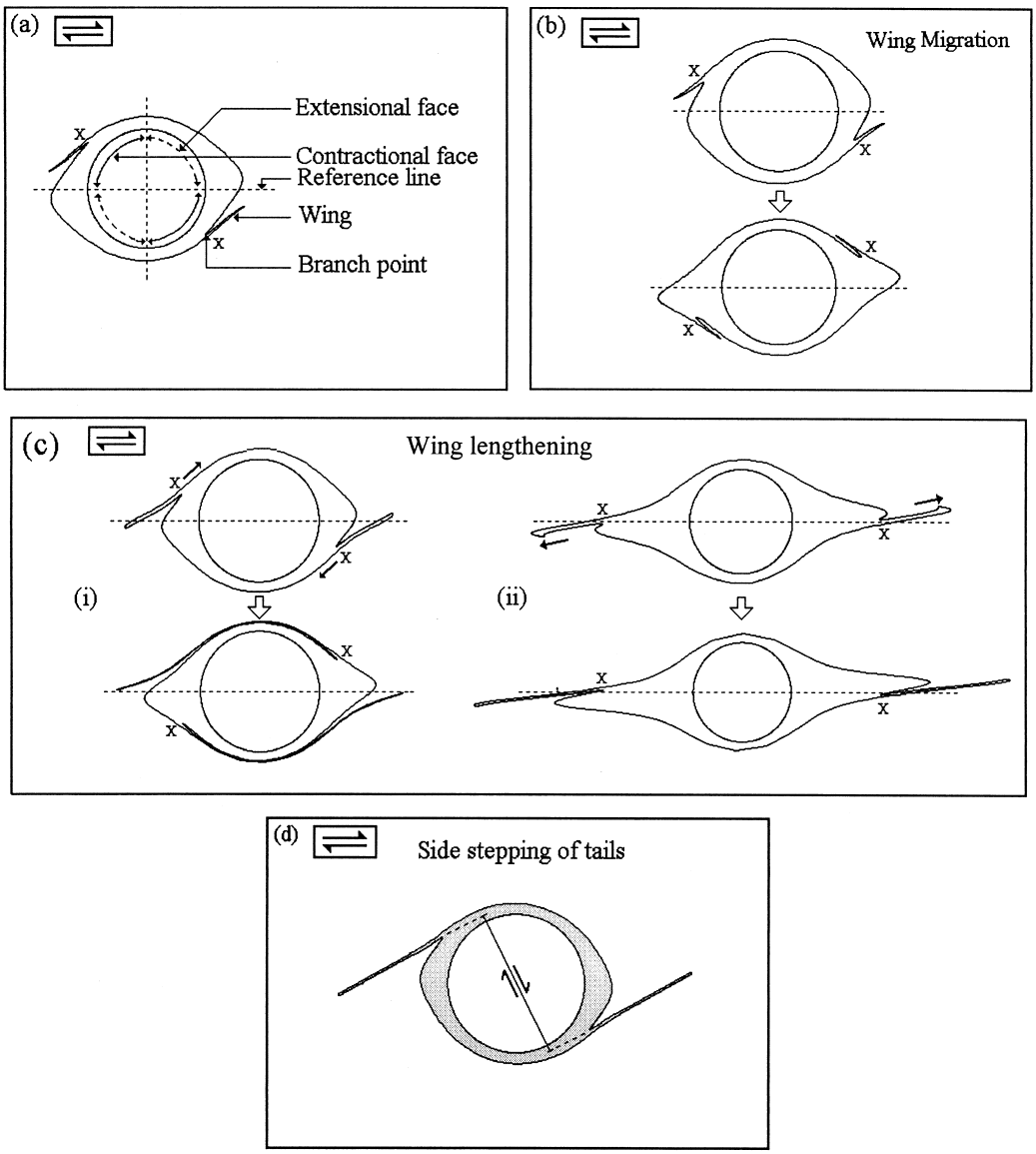

Fig. 2. Diagrammatic representation of the terminologies used in the text. (a) Geometrical terms (see text for details); (b) wing migration by shifting of branch points (X); (c) wing lengthening by two modes: (i) shifting of branch points (X) without wing stretching, (ii) stretching of wings without branch point (X) shifting; (d) side stepping in tail structure.

the instantaneous shortening quadrants of flow which appear as offshoots of a newer generation ϕ-type tails (II in Fig. 3a) in the instantaneous extension quadrants. With further deformation the first generation (I) wings migrate in the shear direction, and eventually coalesce with the growing second generation ϕ-type tails at the extensional faces, giving rise to a hook-like geometry (at $\gamma = 15$ in Fig. 3a). When the bulk finite strain is larger, the hook-form of the tail is engulfed by the growing ϕ-type tails from which newer δ-type wings (third generation—III), offshoot in the contraction quadrants, resulting a complex ϕ–δ mantle structure, as documented by Passchier and Simpson (1986). With further increase in finite strain ($\gamma > 20$), the third generation wings lengthen by branch point shifting in the shear direction without stretching, forming a complex rolled δ-structure as predicted by Masuda and Mizuno (1996). After a large finite strain ($\gamma = 30$), the wings in the mantle are overshadowed by the growing second-generation ϕ-type tails in the extensional quadrant.

The development of mantle structures around porphyroclasts reducing in size at a higher rate ($\dot{R}_a = \dot{R}_b = 0.25$) begins with a δ-type tail as in the earlier model, but subsequently follows a different course as shown in Fig. 3(b). At $\gamma = 30$ the overall mantle structure shows a ϕ-type geometry with δ-type wings (cf. figure 12, ten Brink and Passchier, 1995).

With further increase in the rate of clast-size reduction ($\dot{R}_a = 0.50$), the models show a similar progressive transition from δ-type to δ–ϕ type geometry (Fig. 4a). However, in this model the second-generation tails grow faster and at a certain stage exceed the length of first-generation wings. The first-generation wings lengthen by branch point shifting in the shear direction without stretching (Fig. 4a). The mantle

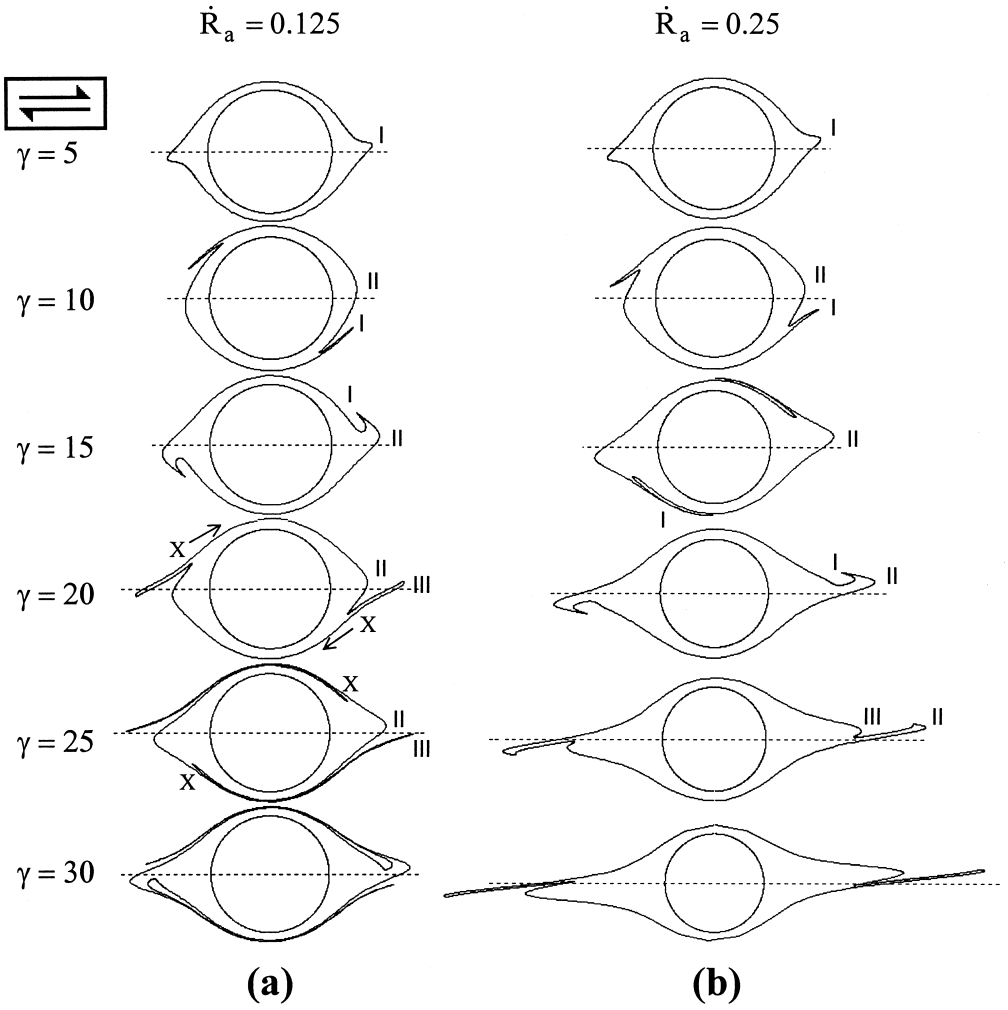

Fig. 3. Successive stages of development of mantle structures around equant porphyroclasts during progressive, dextral simple shear for clast-size reduction rates, (a) $\dot{R}_a = 0.125$ and (b) $\dot{R}_a = 0.25$. I, II, III: first, second and third generations of tail structures. X: branch points of wings. γ: finite bulk shear. Bulk shear rate (γ_b) = 0.025 s^{-1}. Initial mantle width/initial radius of porphyroclast = 0.2. Dashed line represents the reference line parallel to the shear direction and passing the center of the porphyroclast (cf. Passchier and Simpson, 1986).

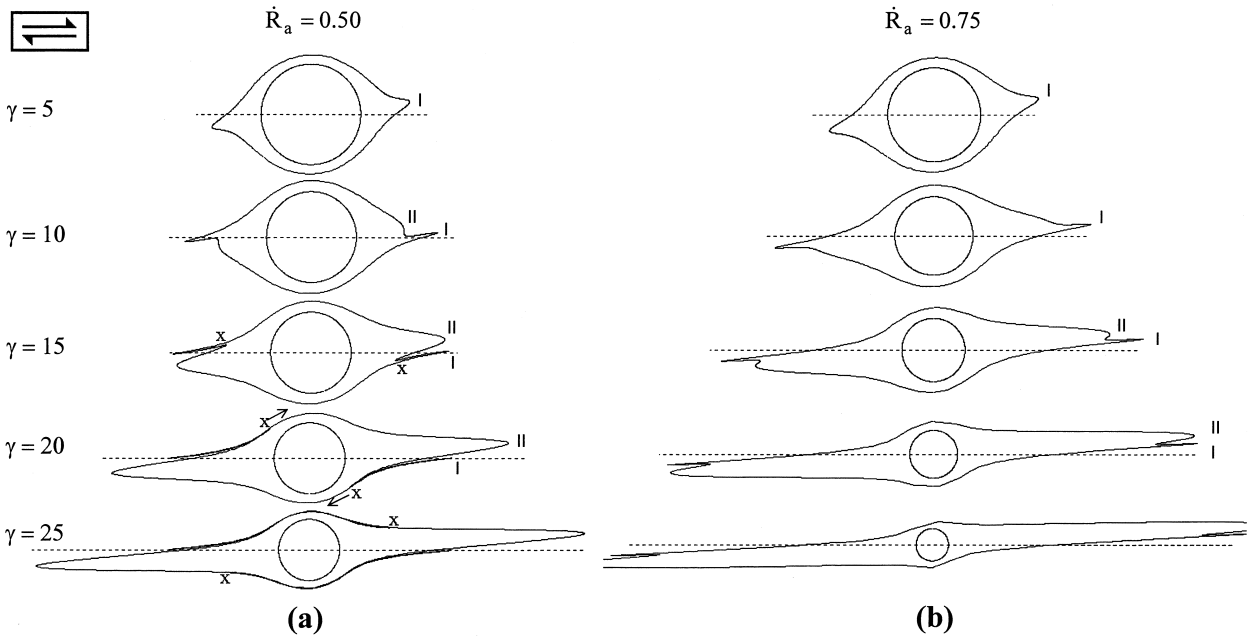

Fig. 4. Successive stages of development of mantle structures around equant porphyroclasts during progressive, dextral simple shear for clast-size reduction rates, (a) $\dot{R}_a = 0.50$ and (b) $\dot{R}_a = 0.75$. Legends and all other conditions are same as in Fig. 3. Note: (1) development of δ-type mantle at a low finite shear ($\gamma = 5$) and its transformation into composite δ–ϕ type geometry with increasing finite shear, (2) the branch points (x) on either side of the porphyroclast shift in the shear direction in (a) and (3) development of ϕ-type mantle at low finite shear ($\gamma = 5$) and its transformation into σ-type geometry with short wings at a large finite shear in (b).

structure in the final model is characterized by long ϕ-type tails with shorter wings on either side of the porphyroclast.

Objects with large size-reduction rates ($\dot{R}_a = 0.75$) develop initially ϕ-type tails. With progressive deformation, second-generation tails form rapidly and the first-generation tails appear as wings shooting off from the newer tails (Fig. 4b). Finally the overall mantle structure assumes a σ-type geometry with very short wings. The tendency of the mantle to form successive generations of tails in the course of progressive deformation is greatly reduced with further increase in $\dot{R}_a$. Thus, for large values of $\dot{R}_a$ (> 2) the mantle shows long, simple σ-type tails at larger values of finite strain ($\gamma > 4$; Fig. 5). The tails show stair-stepping in conformity with the bulk shear sense, as demonstrated by Passchier and Simpson (1986). Our results support earlier observations (Passchier and Simpson, 1986; Bjornerud and Zhang, 1995) that σ-type tail structure can form only when the ratio between the rates of recrystallization and bulk shear, and the finite shear are large.

To understand the development of mantle structures under general type of bulk deformation, separate experiments were run with different ratios of flattening and simple shear rates (S_r) for a particular clast-size reduction rate ($\dot{R}_a = 0.125$). The mantle structures that developed at a particular finite stage of bulk shear ($\gamma = 10$) in different experiments were then compared to investigate the influence of rotationality (W_k) of bulk deformation. The following variations are noticed with decrease in W_k (Fig. 6). (1) The median line of the ϕ-type tails, tends to be at a lower inclination with the shear plane, and may show a reverse inclination at a low value of W_k. (2) The wings in the tail tend to stretch opposite to the bulk shear direction and apparently defining a δ-like geometry. But unlike the typical δ geometry, as defined by Passchier and Simpson (1986), they do not cross the central reference plane.

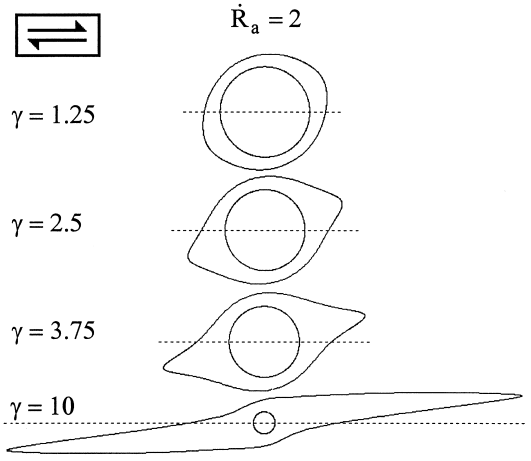

Fig. 5. Development of simple σ-type tails in the mantle during progressive shear at a high rate of clast-size reduction ($\dot{R}_a = 2$). Bulk shear rate (γ_b) = 0.025 s^{-1}.

However, the tails show dextral side-stepping as defined in Fig. 2. (3) At $W_k = 0.75$, the mantle structure assumes a simple geometry (Fig. 6) and appears similar to δ objects without stair stepping described by Passchier et al., 1993.

3.2. Porphyroclasts with moderate aspect ratio (a/b = 1.5)

This set of tests reveals the effects of the shape of porphyroclasts on the structure of their mantles. A series of simulations was made with the long axis of the porphyroclast (initial aspect ratio = 1.5) parallel to the shear direction. The bulk shear rate in the model was fixed as 0.025 s^{-1}. The rates of clast-size reduction along the axial directions of the object were assumed to be equal ($\dot{R}_a = \dot{R}_b = 0.125$). At the initial stage of deformation, incipient tails develop along the long axis of the porphyroclast, while on the contractional faces the mantle deforms into step-like irregularities (Fig. 7a). With progressive deformation they grow, and eventually come closer to each other, forming a double-winged δ-type mantle. Subsequently, the wings experience a drag and increase in length mainly by branch point shifting without significant wing stretching (Fig. 2c), as the long axis of the porphyroclast enters the extension field. At this stage ($\gamma = 12.5$) incipient second-generation, ϕ-type tails form in the extension field. Finally, the mantle shows later generation ϕ-type tails with earlier generation δ-like wings. These types of composite mantle structures have been observed around porphyroclasts in experiments (ten Brink and Passchier, 1995; Passchier, 1999, personal communication).

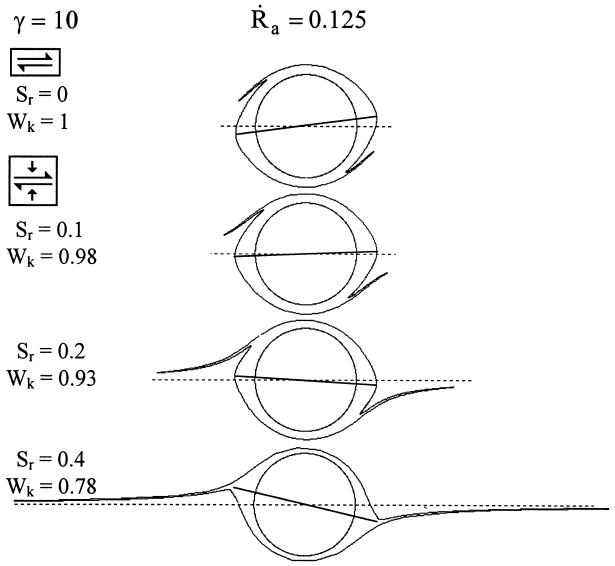

Fig. 6. Variation of mantle structure with increasing rotationality of bulk deformations by a combination of dextral shear and flattening across the shear direction. S_r: the ratio of the rates of flattening and shear. W_k: kinematic vorticity number of bulk deformation. Note that, with decrease of vorticity (1) the median line of ϕ-type tails (solid line) in the mantle lowers the inclination with the shear direction, and finally reverses the sense of inclination with the shear direction, and (2) wings tend to lengthen and dominate the mantle structure and finally, the mantle structures define δ-like geometry without stair stepping.

At a higher rate of clast-size reduction ($\dot{R}_a = 0.25$, Fig. 7b) the mantle structure develops in a similar manner. But in contrast to the earlier model, the first generation wings increase in length by a combination of branch point shifting and wing stretching. As a result, the wings cross the reference plane, forming a typical δ-type geometry. The final pattern consists of later-generation ϕ-type tails with early-formed δ-type wings.

As $\dot{R}_a$ is increased further to 0.5, the mantle structure develops principally by wing stretching without branch point shifting (Fig. 7c). At the initial stage the pattern resembles the double-winged mantle, shown in figure 12(b) of ten Brink and Passchier (1995). With progressive deformation successive generations of wings develop giving rise to a complex multi-winged mantle structure where first generation wings define typical δ-type geometry with stair-stepping.

With further increase in $\dot{R}_a$, the objects do not develop δ-type tails at any stage of progressive deformation. The mantle at a large finite shear shows a σ-type geometry with several generations of ϕ-type wings (Fig. 8a). With progressive deformation the wings increase in length by stretching and rotate towards the shear plane. The tendency of objects to form multi-generation wings declines as $\dot{R}_a$ is further increased. At a high rate of clast-size reduction ($\dot{R}_a = 5$) the mantle develops a simple σ-type tail (Fig. 8b).

To investigate the effect of rotationality of bulk deformation (W_k) we followed the same procedure as stated in Section 3.1. The experiments were run with the long axis of the porphyroclast (a/b = 1.5) initially parallel to the shear plane up to a finite bulk shear ($\gamma = 5$). With increase in S_r, i.e. decrease in W_k of the bulk deformation, the ϕ-type tails that grow near the long axis of the porphyroclast tend to die out, whereas the wings on the contractional faces become more and more dominant, and tend to attain a δ-like geometry (Fig. 9). However, unlike the typical δ geometry, they do not cross the reference plane. However, the wings show dextral side-stepping as defined in Fig. 2. At $W_k = 0.78$, the mantle structure appears similar to δ objects without stair stepping described by Passchier et al. (1993) (Fig. 9).

3.3. Porphyroclasts with large aspect ratio (a/b = 3)

Porphyroclast mantle development was also modeled with clasts of aspect ratio 3 under the same conditions

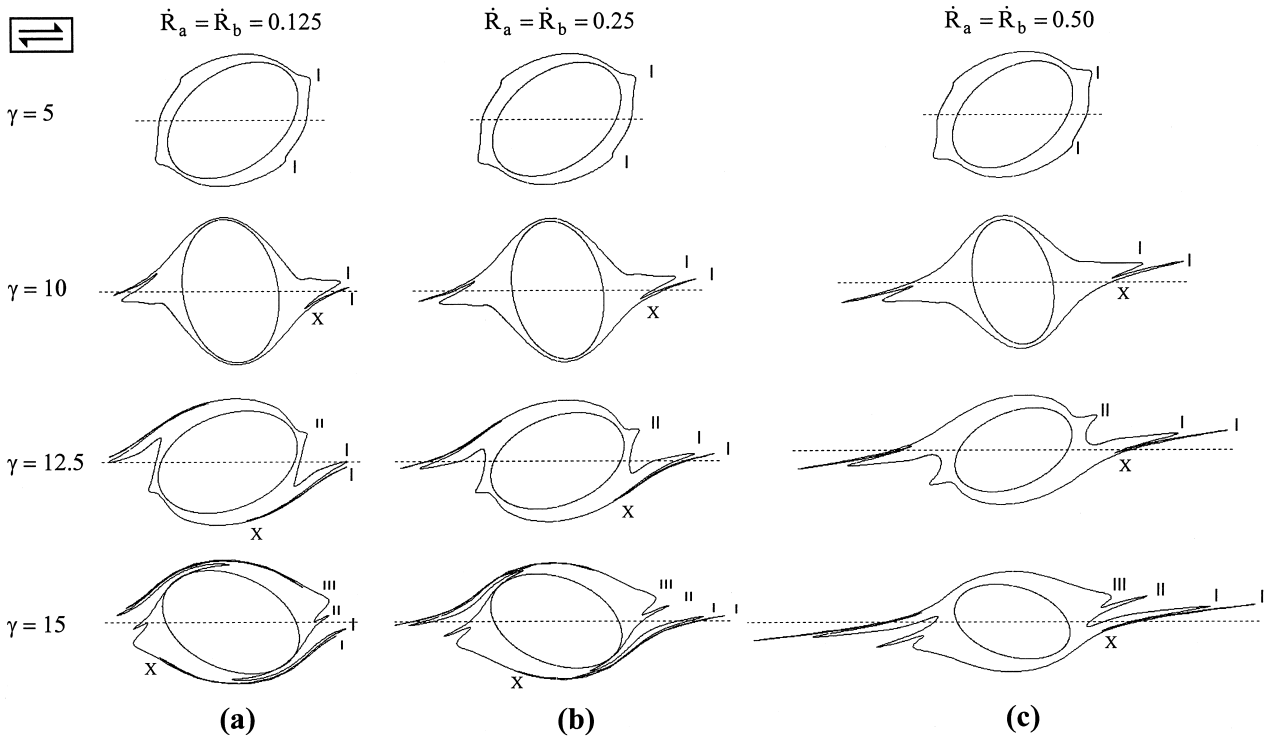

Fig. 7. Successive stages of development of mantle structures around inequant porphyroclasts (initial aspect ratio = 1.5) during progressive, dextral simple shear for clast-size reduction rates, $\dot{R}_a = \dot{R}_b = 0.125$, 0.25 and 0.50 in (a), (b) and (c), respectively. The long axes of the porphyroclasts were initially parallel to the shear direction. Legends and other conditions are same as in Fig. 3. Note: (1) development of composite rolled δ–ϕ structures in (a), (2) wings run across the reference line (dashed) at higher rates of size reduction, forming a typical δ-type geometry in (b) and (c).

as described in the previous section. The tail patterns are somewhat different from those produced in earlier models. At the initial stage δ-like tails form close to the long axis of the porphyroclast, and as the latter rotates across the contraction field the tails are continuously dragged away developing a large side stepping with a sense consistent with that of the bulk shear (Fig. 10a). Second-generation ϕ-type tails form and the first generation tails appear as wings when the porphyroclast comes into the extension field. The overall pattern is very similar to overturned porphyroclast systems (figure 6h of Passchier and Simpson, 1986).

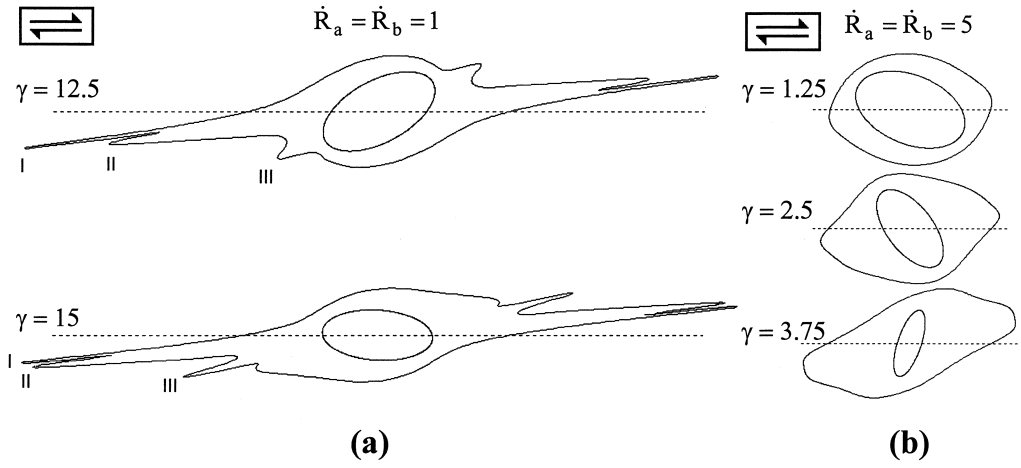

Fig. 8. Successive stages of development of mantle structures around inequant porphyroclasts (initial aspect ratio = 1.5) during progressive, dextral simple shear for clast-size reduction rates, $\dot{R}_a = \dot{R}_b = 1$ and 5 in (a) and (b), respectively. The long axes of the porphyroclasts were initially parallel to the shear direction. Legends and other conditions are same as in Fig. 3. Note: (1) transition of the overall mantle structure from ϕ-type to σ-type during progressive shear in (a) and (2) development of typical σ-type tails under higher clast-size reduction rate in (b).

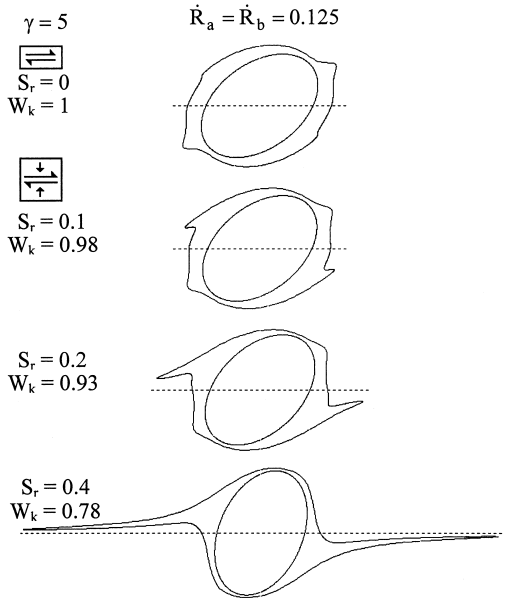

Fig. 9. Geometrical variation of mantle pattern with increasing rotationality (W_k) of bulk deformation by a combination of dextral simple shear and flattening across the shear direction. Legends are same as in Fig. 6. The aspect ratio and the long axis of porphyroclast were initially 1.5 and parallel to the shear direction, respectively. Note development of δ-like tails without stair stepping at $W_k = 0.78$.

Our simulation indicates that this pattern can develop only when the porphyroclasts are of a large aspect ratio. During progressive deformation the wings migrate in the shear direction and get distorted due to development of second-generation tails in the extension quadrant. As $\dot{R}_a$ is increased, the tendency of wing migration declines, and the wings lengthen by branch point shifting in the shear direction. The mantle finally shows ϕ-type tails with δ-like wings (Fig. 10b), as observed in natural porphyroclasts (e.g. figure 6g of Passchier and Simpson, 1986).

To investigate the effects of rotationality of bulk deformation (W_k) we followed the same procedure as stated in Section 3.2. Two sets of experiments were run with the long axis of the porphyroclast ($a/b = 3$) initially parallel and perpendicular to the shear plane. The mantle structure of porphyroclasts initially parallel to the shear direction changes from a composite pattern to simple δ-like tails with decrease in vorticity number W_k (Fig. 11a). Porphyroclasts initially at right angles to the shear direction develop typical δ tails at higher values of W_k, which transforms into an atypical δ-like pattern with decrease in W_k (Fig. 11b). The sense of side stepping of the tails in both the cases, however, is consistent with the sense of bulk shear (Fig. 11).

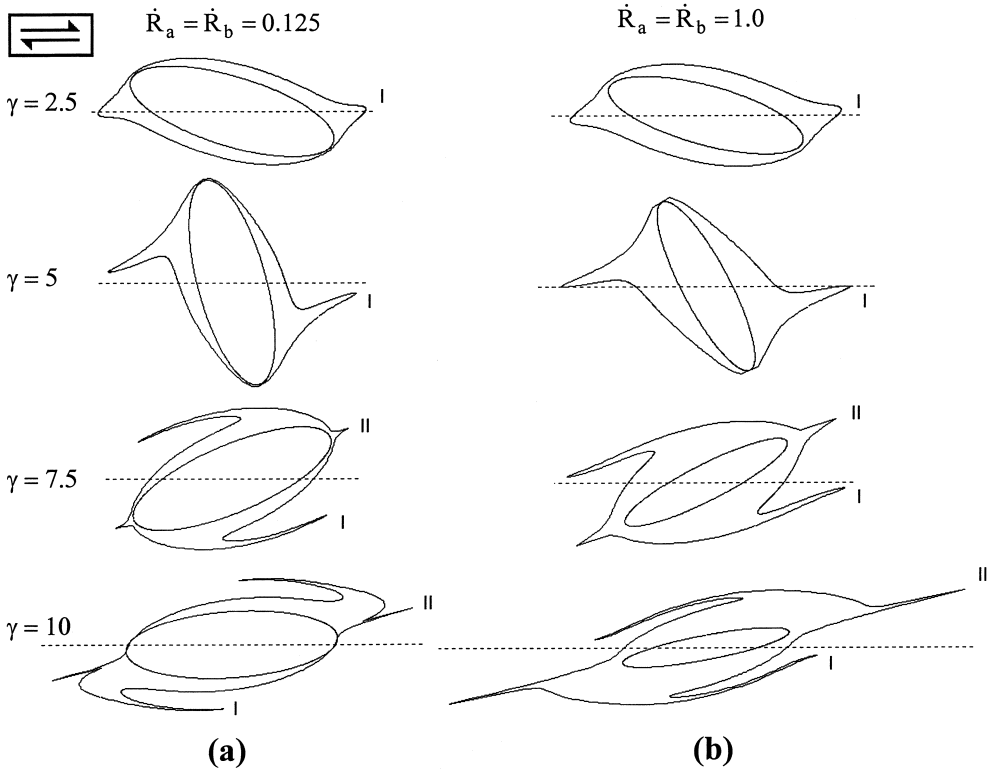

Fig. 10. The patterns of (δ-type) mantle structures around porphyroclasts of high initial aspect ratio (3) for different clast-size reduction rates. Legends and other conditions are same as in Figs. 3 and 7. Note overturned δ-structures at large shear. The long axis of the porphyroclast was initially parallel to the shear direction.

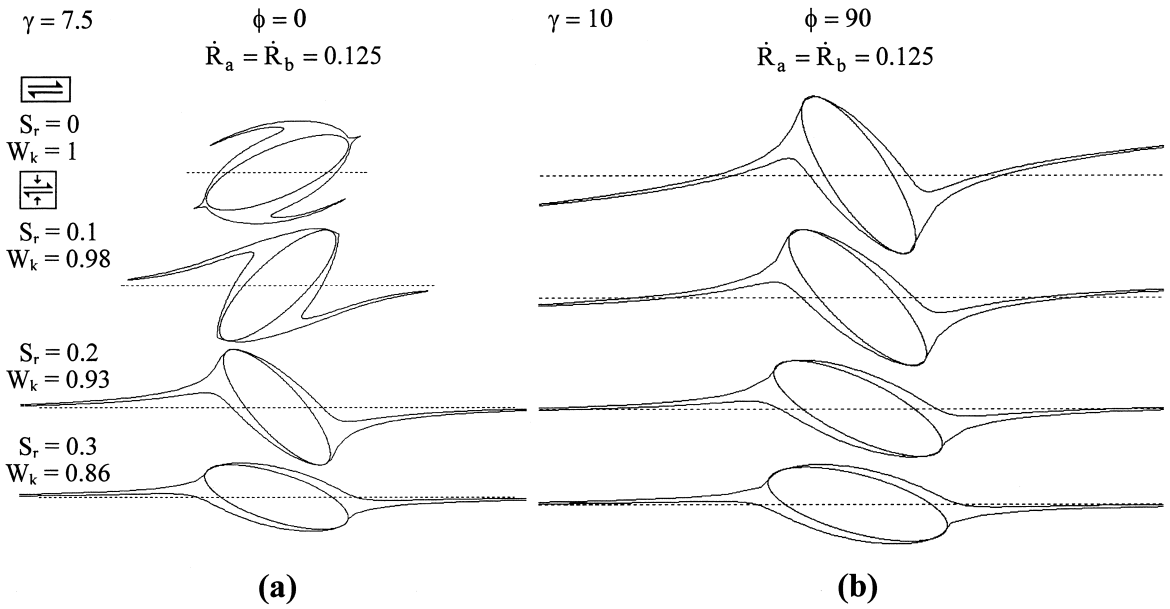

Fig. 11. Geometrical variation of mantle pattern with increasing rotationality (W_k) of bulk deformation by a combination of dextral simple shear and flattening across the shear direction. The initial aspect ratio of porphyroclasts was 3. The long axes of porphyroclasts in (a) and (b) were initially parallel and perpendicular to the shear direction, respectively. Legends are same as in Fig. 6.

4. Discussion

Our numerical models develop δ-, ϕ- and finally σ-type mantle structures (Passchier, 1994) as the rate of clast-size reduction is increased. The Masuda and Mizuno (1996) model is similar to our model, but they did not produce the σ-type. This difference is probably due to the difference in modeling of object size in progressive deformation. In our model the object continuously reduces in size during progressive deformation, adding new material to the mantle, while in their model the objects have a fixed dimension throughout the course of deformation. In fact our results qualitatively conform to the model of Bjornerud and Zhang (1995) that shows the development of σ-type objects at a high rate of recrystallization. Similar results were also obtained from analog model experiments (Passchier and Simpson, 1986). For a given rate of clast-size reduction the mantle geometry changes with increasing finite shear strain during progressive deformation. The stability fields of the principal mantle types have been delimited in the space of finite strain vs. recrystallization rate from physical and numerical model experiments (Passchier and Simpson, 1986; Bjornerud and Zhang, 1995). These studies are, however, restricted to a moderate finite strain ($\gamma \leq 10$). Our simulations and those of Masuda and Mizuno (1996) show development of complex, but definite patterns for larger finite strains. We present a broader field diagram (Fig. 12) including these complex patterns.

The study reveals that typical δ-type tails that cross the reference plane and show stair stepping generally develop for moderate rates of clast-size reduction (0.25–0.5). When the rate of clast-size reduction is lower, the mantle structure looks like incipient δ-type tails that do not cross the reference plane, which at lower values of W_k appear as δ objects without stair stepping (Passchier et al., 1993).

Our analysis demonstrates the control of the initial shape on the geometry of mantle structures. For the same kinematic and physical conditions, porphyroclasts of different initial shapes develop different patterns in their mantles (Fig. 13). At a low finite strain, elongate objects with larger aspect ratio have more complex multiwinged tail patterns in comparison to those of equant objects, except at higher values of clast-size reduction rate. In natural mylonites the former may be mistaken to represent high finite shear. Such a qualitative assessment of finite strain from mantle structures may thus be erroneous unless other factors are taken into account.

The ratio of the flattening and simple shear rates in shear zones can be an additional factor in controlling the mantle structures of porphyroclasts. In our simulations, with increase in the value of this ratio (i.e. decrease in kinematic vorticity number W_k in the bulk deformation), porphyroclasts tend to form simple tails. However, we performed these numerical experiments with the long axis of the porphyroclast either parallel or perpendicular to the shear direction, and further investigation is necessary to demonstrate if such a relationship holds for any initial orientation of the porphyroclast with the shear direction.

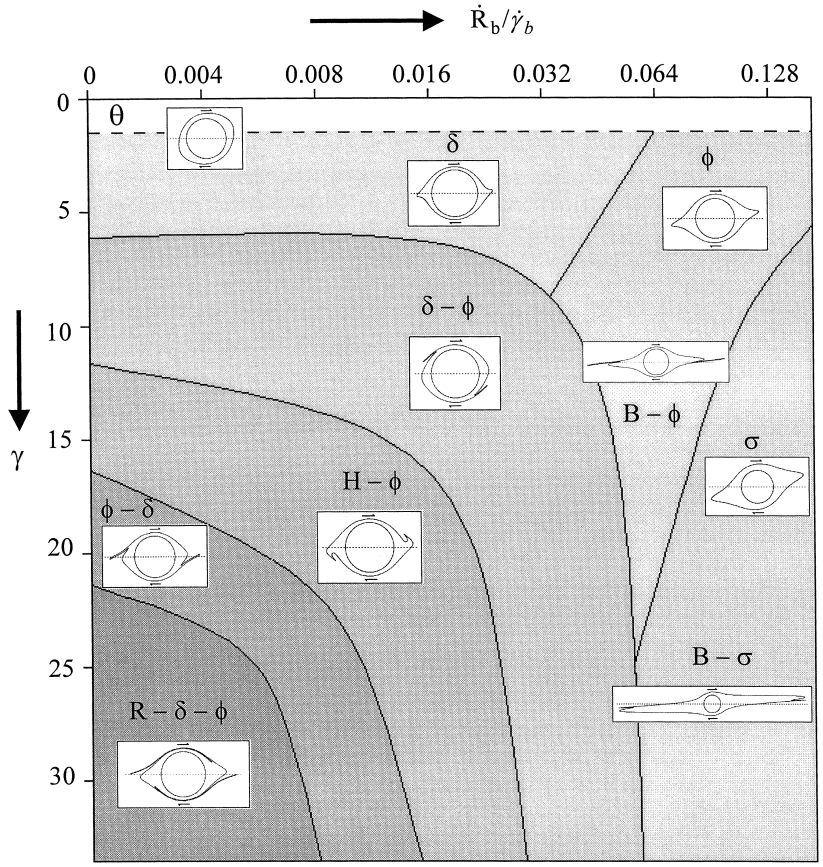

Fig. 12. A generalized diagram representing fields of typical mantle patterns in the space of size-reduction rate (normalized to the bulk shear rate) vs. finite bulk shear. δ–ϕ: ϕ tail with incipient δ wing; $\phi\delta$: combination of ϕ- and δ-type geometry; H–ϕ: hooked ϕ; R–δ–ϕ: rolled δ–ϕ; B–ϕ: branched ϕ; B–σ: branched σ.

Porphyroclast systems are very useful shear sense indicators (Passchier and Trouw, 1996). The rotation of an equant object takes place with a uniform angular velocity, while an inequant object rotates with a changing velocity. In the latter case the object may even rotate with a sense opposite to the shear sense where a flattening component acts across the shear zone (Passchier, 1987). An obvious doubt then arises on the usage of tail patterns of elongate porphyroclasts as shear sense indicators. In our numerical models, inequant objects show more complex patterns containing multiple wings. However, the wings on either side of the object are generally arranged with a significant side stepping and the sense of side stepping is synthetic to the bulk shear sense (Fig. 7). Elongate porphyroclasts with multiwinged mantles can thus probably be used for the determination of shear sense in shear zones. Our simulations, however, were performed with the long axis of the porphyroclast either at right angles or parallel to the shear direction. The utility of tail patterns of elongate porphyroclasts as shear sense indicators thus needs to be investigated further by considering different initial orientations of the porphyroclasts.

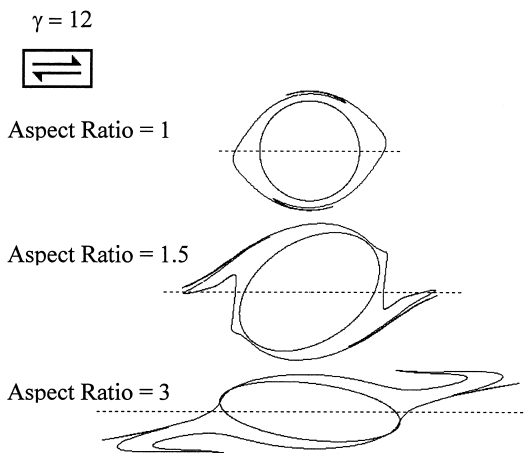

Fig. 13. Variation in the pattern of mantle structure with increase in aspect ratio of porphyroclast, when all other factors remain constant.

The present analysis assumes a Newtonian rheology of the matrix. Earlier studies (Passchier, 1994) indicate that the geometry of porphyroclast tails is sensitive to the matrix rheology (e.g. non-Newtonian behavior). In addition, Bjornerud and Zhang (1995) and Ildefonse

and Mancktelow (1993) showed that the degree of coupling between the object and matrix is also a controlling factor. Moreover, this analysis is two-dimensional, considering plane strain type of bulk deformation with the rotation axis of porphyroclast along the direction of no-strain. The motion of ellipsoidal porphyroclasts in three-dimensions is complex when the long axis is at angles to the orthogonal instantaneous stretching axes of the flow (Passchier, 1987). The numerical experiments described here mostly consider porphyroclasts initially aligned parallel to the shear direction with a few at right angles and thus do not reveal the effects of initial orientation on the development of mantle structure (cf. Simpson and De Paor, 1993). The present study is thus much simplified and only shows the probable effects of the initial shape of the porphyroclast, the rate of clast-size reduction and the rotationality of bulk deformation on the geometry of mantle structures. In spite of such a simplistic approach, the mantle structures produced in the numerical experiments conform to those of physical test models and natural mylonites.

5. Conclusions

At a low finite strain, equant objects develop simple δ-type tails, which are replaced by ϕ-type as the rate of clast-size reduction is increased. σ-type tails form at a high rate of clast-size reduction and a high finite strain. With an increase in finite shear strain, the tails tend to have successive generations of wings forming complex mantle structures except for at a very high rate of clast-size reduction. Elongate objects may develop composite tail patterns consisting of multiple wings, even at low finite strains and the mantle structures become increasingly complex with increase in aspect ratio. For a given finite shear, decrease in the vorticity of bulk deformation leads to development of simpler mantle structures and vice-versa.

Acknowledgements

We wish to thank Professors C. Passchier and K. Schulmann for their detailed insightful comments on the manuscript. Dr. R.J. Lisle is thanked for giving us an outline for revising the manuscript. We are grateful to Professors C. Simpson, D. De Paor, and G. Mitra for their helpful comments and suggestions on an early version of the manuscript. Dr. J. Jezek is specially thanked for checking the mathematical part of the manuscript. The present work was carried out under a project of DST, India sanctioned to NM. CC acknowledges the infrastructural facilities provided by the Indian Statistical Institute, Calcutta.

Appendix A

In this section we give derivations of the parameters and constants of the velocity functions in Eqs. (10a) and (10b). The velocity components at a point in the neighborhood of an object can be defined in two-dimension [cf. equations (22) and (23) of Jeffery, 1922] as:

$$\begin{aligned} u' =& \left[S'_{11} - 2A_1(\alpha+\beta) - F_1\gamma\right]x' \\ &+ \left[S'_{12} - 2(\alpha D_1 - \beta C_1) + E_1\gamma\right]y' \\ &- \frac{2x'P^2}{(a+\lambda)\Delta}\left[\left\{E_1 + 2(a^2+\lambda)C_1 + 2(b^2+\lambda)D_1\right\}\right. \\ &\left.\times \frac{1}{(a^2+\lambda)(b^2+\lambda)}x'y'\right] \\ &- \frac{2x'P^2}{(a+\lambda)\Delta}\left[\left\{F_1 - 2(a^2+\lambda)A_1 + 2(b^2+\lambda)B_1\right\}\right. \\ &\left.\times \frac{1}{(b^2+\lambda)^2}y'^2\right] \end{aligned} \tag{A1a}$$

$$\begin{aligned} v' =& \left[S'_{22} - 2B_1(\alpha+\beta) - F_1\gamma\right]y' \\ &+ \left[S'_{21} - 2(\alpha D_1 - \beta C_1) + E_1\gamma\right]x' \\ &- \frac{2y'P^2}{(b^2+\lambda)\Delta}\left[\left\{E_1 + 2(a^2+\lambda)C_1 + 2(b^2+\lambda)D_1\right\}\right. \\ &\left.\times \frac{1}{(a^2+\lambda)(b^2+\lambda)}x'y'\right] \\ &+ \frac{2y'P^2}{(b^2+\lambda)\Delta}\left[\left\{F_1 - 2(a^2+\lambda)A_1 + 2(b^2+\lambda)B_1\right\}\right. \\ &\left.\times \frac{1}{(a^2+\lambda)^2}x'^2\right] \end{aligned} \tag{A1b}$$

where,

$$\Delta = \sqrt{(a^2+\lambda)(b^2+\lambda)} \text{ and } \frac{1}{P^2} = \frac{x'^2}{(a^2+\lambda)^2} + \frac{y'^2}{(b^2+\lambda)^2}.$$

α, β, and γ in Eqs. (A1a) and (A1b) are geometric parameters. In two dimensions their expressions are:

$$\begin{aligned} &\alpha = \int_\lambda^\infty \frac{\mathrm{d}\,\lambda}{(a^2+\lambda)\Delta},\ \beta = \int_\lambda^\infty \frac{\mathrm{d}\,\lambda}{(b^2+\lambda)\Delta} \\ &\text{and } \gamma = \int_\lambda^\infty \frac{\mathrm{d}\,\lambda}{(a^2+\lambda)(b^2+\lambda)\Delta} \end{aligned} \tag{A2}$$

where $\Delta = \sqrt{(a^2+\lambda)(b^2+\lambda)}$. One of the most important steps in finding the solution of the velocity field is to solve out the integration in Eq. (A2). This can be

made in the following way:

$$\alpha = \int_k^{\infty} \frac{\mathrm{d}\,\lambda}{(a^2+\lambda)\Delta}.$$

Let $Z=(b^2+\lambda)^{1/2}$ and have,

$$\alpha = \int_{\sqrt{b^2+k}}^{\infty} \frac{2\mathrm{d}\,Z}{(Z^2+A^2)^{3/2}}, \text{ where } A^2 = a^2 - b^2.$$

We again substitute $Z=A\tan\theta$ and get,

$$\alpha = \frac{2}{A^2}\int_{\tan^{-1}} \left(\frac{\sqrt{b^2+k}}{A}\right)^{\frac{\pi}{2}} \cos\theta\,\mathrm{d}\,\theta,$$

which gives rise to:

$$\alpha = \frac{2}{a^2-b^2}\left[1-\sin\left\{\tan^{-1}\left(\frac{b^2+k}{A}\right)\right\}\right]$$

Substituting A and k by (a^2-b^2) and λ, respectively, and after some algebra, we have

$$\alpha = \frac{2}{a^2-b^2}\left[\frac{\sqrt{a^2+\lambda}-\sqrt{b^2+\lambda}}{\sqrt{a^2+\lambda}}\right]. \tag{A3a}$$

Following the same steps, we get

$$\beta = \frac{2}{a^2-b^2}\left[\frac{\sqrt{a^2+\lambda}-\sqrt{b^2+\lambda}}{\sqrt{b^2+\lambda}}\right] \tag{A3b}$$

$$\gamma = \frac{2}{(a^2-b^2)^2}\left[\frac{\left(\sqrt{a^2+\lambda}-\sqrt{b^2+\lambda}\right)^2}{\sqrt{(a^2+\lambda)(b^2+\lambda)}}\right]. \tag{A3c}$$

It may be noted that α, β, γ in Eqs. (A3a), (A3b) and (A3c) tend to be zero as $\lambda=\infty$, and thereby Eqs. (A1a) and (A1b) give rise to velocity components as in Eq. (4). Eqs. (A1a) and (A1b) contain six unknowns, which will be determined by imposing boundary conditions. If the instantaneous rotation rate of the object is ω, the velocity of a point on the surface of object, $\lambda=0$ will be:

$$u_s' = -\omega y' \text{ and } v_s' = \omega x'. \tag{A4}$$

Substituting $\lambda=0$ in Eq. (A1a) and comparing then with Eq. (A4), we can form following equations:

$$S_{11}' + F_1\gamma_0 - 2A_1(\alpha_0+\beta_0) = 0 \tag{A5a}$$

$$S_{12}' + E_1\gamma_0 + 2(\alpha_0 D_1 - \beta_0 C_1) = -\omega \tag{A5b}$$

$$E_1 + 2a^2C_1 + 2b^2D_1 = 0 \tag{A5c}$$

$$F_1 - 2a^2A_1 + 2b^2B_1 = 0 \tag{A5d}$$

$$S_{21}' + E_1\gamma_0 - 2(\alpha_0 D_1 - \beta_0 C_1) = \omega \tag{A5e}$$

$$S_{22}' - F_1\gamma_0 - 2B_1(\alpha_0+\beta_0) = 0. \tag{A5f}$$

Now, solving six equations Eq. (A5a–f) we get the coefficients in terms of known quantities.

$$A_1 = \frac{S_{11}'}{2\left[(\alpha_0+\beta_0)-(a^2+b^2)\gamma_0\right]},$$

$$B_1 = -\frac{S_{11}'}{2\left[(\alpha_0+\beta_0)-(a^2+b^2)\gamma_0\right]},$$

$$C_1 = \frac{\alpha_0\frac{1}{2}(S_{12}'+S_{21}') - \gamma_0 b^2\left(\frac{1}{2}(S_{21}'-S_{12}')-\omega\right)}{2(\alpha_0 a^2+\beta_0 b^2)\gamma_0},$$

$$D_1 = \frac{\beta_0\frac{1}{2}(S_{12}'+S_{21}') + \gamma_0 a^2\left(\frac{1}{2}(S_{21}'+S_{12}')-\omega\right)}{2(\alpha_0 a^2+\beta_0 b^2)\gamma_0},$$

$$E_1 = -\frac{\frac{1}{2}(S_{12}'+S_{21}')}{\gamma_0},$$

$$F_1 = \frac{S_{11}'(a^2+b^2)}{(\alpha_0+\beta_0)-(a^2+b^2)\gamma_0}. \tag{A6}$$

Substituting $\lambda=0$ in Eqs. (A3a), (A3b) and (A3c), we get

$$\alpha_0 = \frac{2}{a(a+b)},\ \beta_0 = \frac{2}{b(a+b)}$$
$$\text{and } \gamma_0 = \frac{2}{ab(a+b)^2}. \tag{A7}$$

From equation (37) of Jeffery (1922) we have,

$$\omega = \frac{a^2S_{21}' - b^2S_{12}'}{a^2+b^2} \tag{A8}$$

The constants in Eq. (A6) are now obtained in terms of known quantities. We substitute them in Eqs. (A1a) and (A1b), and after some algebra have the expressions in Eqs. (10a) and (10b).

References

Bjornerud, M., 1989. Toward a unified conceptual framework for shear-sense indicators. Journal of Structural Geology 11, 1045–1049.

Bjornerud, M.G., Zhang, H., 1995. Flow mixing object matrix coherent mantle growth and the development of porphyroclast tails. Journal of Structural Geology 17, 1347–1350.

Choukroune, P., Gapais, D., Merle, O., 1987. Shear criteria and structural symmetry. Journal of Structural Geology 9, 525–530.

Ghosh, S.K., Ramberg, H., 1976. Reorientation of inclusions by combination of pure shear and simple shear. Tectonophysics 34, 1–70.

Ghosh, S.K., 1987. Measure of non-coaxiality. Journal of Structural Geology 9, 111–113.

Hanmer, S., Passchier, C.W., 1991. Shear sense indicators: a review. Geological Survey of Canada Paper 90, 1–71.

Hooper, R.J., Hatcher, R.D., 1988. Mylonites from the Towaliga fault zone, central Georgia: products of heterogeneous non-coaxial deformation. Tectonophysics 152, 1–17.

Ildefonse, B., Mancktelow, N.S., 1993. Deformation around rigid particle: influence of slip at the particle/matrix interface. Tectonophysics 221, 345–359.

Jeffery, G.B., 1922. The motion of ellipsoidal particles immersed in a viscous fluid. Proceedings of the Royal Society of London A 120, 161–179.

Jezek, J., Saic, S., Segeth, K., Schulmann, K., 1999. Three-dimensional hydrodynamical modelling of viscous flow around a rotating ellipsoidal inclusion. Computers and Geosciences 25, 547–558.

Lamb, H., 1932. Hydrodynamics. Cambridge University Press, Cambridge.

Masuda, T., Mizuno, N., 1996. Computer modeling of mantled porphyroclasts in Newtonian and non-Newtonian simple shear viscous flows. Journal of Structural Geology 18, 1487–1491.

Mawer, C.K., 1987. Shear criteria in the Greenville Province, Ontario, Canada. Journal of Structural Geology 9, 531–539.

Passchier, C.W., Simpson, C., 1986. Porphyroclast systems as kinematic indicators. Journal of Structural Geology 8, 831–844.

Passchier, C.W., 1987. Stable positions of rigid objects in non-coaxial flow: a study in vorticity analysis. Journal of Structural Geology 9, 679–690.

Passchier, C.W., ten Brink, C.E., Bons, P.D., Sokoutis, D., 1993. δ objects as a gauge for stress sensitivity of strain rate in mylonites. Earth and Planetary Science Letters 120, 239–245.

Passchier, C.W., Sokoutis, D., 1993. Experimental modeling of mantled porphyroclasts. Journal of Structural Geology 15, 895–910.

Passchier, C.W., 1994. Mixing in flow perturbations: a model for development of mantle porphyroclasts in mylonites. Journal of Structural Geology 16, 733–736.

Passchier, C.W., Trouw, R.A.J., 1996. Microtectonics. Springer, Berlin, p. 289.

Simpson, C., De Paor, D., 1993. Strain and kinematic analyses in general shear zones. Journal of Structural Geology 15, 1–20.

ten Brink, C.E., Bons, P.D., Passchier, C.W., 1993. Approximate stream functions for flow around rigid objects in shear zones. Abstract supplement to Terra Nova 2, 5–35.

ten Brink, C., Passchier, C.W., 1995. Modeling of mantled porphyroclasts using non-Newtonian rock analogue materials. Journal of Structural Geology 17, 131–146.

Van Der Driessche, J., Brun, J.-P., 1987. Rolling structures at large shear strains. Journal of Structural Geology 9, 691–704.